INTERFEROMETRIC IMAGING AND TIME REVERSAL IN RANDOM MEDIA

LILIANA BORCEA†

Mathematics Subject Classifications: 35Q60, 35Q86, 60G99, 78A48

Short Description. We present a comparative study of time reversal and array imaging in random media. We explain that the time reversal process is fundamentally different than imaging, and it cannot be used for imaging purposes. We also describe briefly the resolution of time reversal and imaging. Since they occur in random media, the resolution theory is augmented with the important concept of statistical stability. It refers to robustness of the processes with respect to different realizations of the random medium.

Description. *Time reversal* is a physical experiment that uses special arrays of transducers, called time reversal mirrors (TRM) [Fink, 1997]. The transducers in a TRM operate as both receivers and sources, as illustrated in Figure 1. First, they record the signals emitted by a remote localized source. Then, they time reverse these signals and re-emit them into the medium. The waves propagate back toward the source and focus near it. In *passive array imaging*, the transducers are only receivers that record the array data, the signals from the localized source. Then, the data are processed numerically to obtain an imaging function evaluated at points $\vec{\mathbf{y}}$ in a search domain. The peaks of this function are the estimates of the source location.

It is often said that any imaging process involves some form of time reversal. This is true in some sense *if imaging occurs in media that are known in detail*. Then, numerical propagation of the waves in our model of the medium resembles closely the physical wave propagation in the true medium. We consider here heterogeneous media, cluttered by inhomogeneities that scatter the waves. They arise in applications like ground or foliage penetrating radar, seismic exploration, shallow water acoustics, nondestructive evaluation of heterogeneous materials like aging concrete, and so on. When imaging in clutter, we know at best the large scale, the smooth features of the medium. If we do not know them, it may be feasible to estimate them using a process called *velocity estimation*, that requires additional data. See for example the semblance velocity estimation approach described in [Carazzone and Symes, 1991], or the travel time tomography approach [Uhlmann, 2001]. However, we cannot know in detail and it is not feasible to estimate the small scale structure of cluttered media, the inhomogeneities. That is to say, there is uncertainty about the clutter, which is why we model it as a random spatial process and speak of imaging in random media.

The time reversal experiment can be carried out without any knowledge of the medium and, surprisingly at first, clutter may improve the wave focusing at the source [Fink, 1997]. Time reversal requires however that we *observe the field at the time of refocus, and in the vicinity of the source*, which is of course not possible in imaging applications. That is to say, *time reversal cannot be used for imaging.* In what follows we describe in detail the fundamental differences between time reversal and imaging in clutter, using the mathematical model of the scalar wave equation with randomly fluctuating wave speed.

1. Mathematical model. The acoustic pressure $p(t,\vec{\mathbf{x}})$ solves the wave equation

$$\frac{1}{c^2(\vec{\mathbf{x}})}\frac{\partial^2 p(t,\vec{\mathbf{x}})}{\partial t^2} - \Delta p(t,\vec{\mathbf{x}}) = F(t,\vec{\mathbf{x}}), \quad \vec{\mathbf{x}} \in \mathbb{R}^n, \quad t > 0, \tag{1.1}$$

in a medium with wave velocity $c(\vec{\mathbf{x}})$, satisfying $c(\vec{\mathbf{x}}) = c_o(\vec{\mathbf{x}})[1 + \gamma\mu(\vec{\mathbf{x}})]$. Here $c_o(\vec{\mathbf{x}})$ is the smooth, mean speed that describes the large scales features of the medium, and $\mu(\vec{\mathbf{x}})$ is a random function that models the inhomogeneities. We assume it to be stationary, with mean $\mathbb{E}\{\mu(\vec{\mathbf{x}})\} = 0$ and with auto-correlation $\mathcal{R}(\vec{\mathbf{x}}) = \mathbb{E}\{\mu(\vec{\mathbf{x}}' + \vec{\mathbf{x}})\mu(\vec{\mathbf{x}}')\}$ normalized by $\mathcal{R}(0) = 1$. The amplitude of the random fluctuations is modeled by the dimensionless parameter γ.

†Computational and Applied Mathematics, Rice University, MS 134, Houston, TX 77005-1892. (borcea@caam.rice.edu)

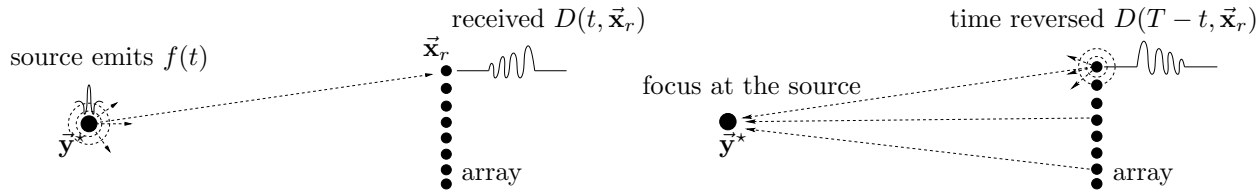

FIG. 1. *Schematic of the time reversal experiment. On the left, we illustrate a localized source that emits a signal $f(t)$. The transducers at locations $\vec{\mathbf{x}}_r$ in the array record the signal $D(t, \vec{\mathbf{x}}_r)$. On the right, we illustrate how the transducers emit the time reversed signal, and how the waves travel back to the source, where they focus.*

We neglect any boundaries in the problem, and suppose that the waves propagate in the whole space $\mathbb{R}^n$, with $n = 2$ or 3. The medium is assumed quiescent $p(t, \vec{\mathbf{x}}) = 0$ before the source excitation, modeled by $F(t, \vec{\mathbf{x}}) = f(t)\rho(\vec{\mathbf{x}})$. Here $f(t)$ is the emitted signal, a short pulse, and $\rho(\vec{\mathbf{x}}) \geq 0$ is the source density, compactly supported in a small ball centered at $\vec{\mathbf{y}}^\star$, and normalized to integrate to one.

1.1. The array and system of coordinates. There are N transducers at locations $\vec{\mathbf{x}}_r$, in a compact set $\mathcal{A}$ on an $n-1$ dimensional surface. They are closely spaced so that they behave as a collective entity, the array. In the analysis, it is usually assumed for simplicity that $\vec{\mathbf{x}}_r$ are uniformly spaced on a mesh of small size h, to allow the continuum approximation

$$h^{n-1} \sum_{r=1}^{N} \varphi(\vec{\mathbf{x}}_r) \approx \int_{\mathcal{A}} ds(\vec{\mathbf{x}})\, \varphi(\vec{\mathbf{x}}). \tag{1.2}$$

Here $ds(\vec{\mathbf{x}})$ is the infinitesimal area of the surface and φ is an arbitrary integrable function. We take for simplicity a planar array, with $\mathcal{A}$ a square of side a for $n = 3$, and $\mathcal{A}$ a line segment of length a for $n = 2$. We call a the *array aperture*.

The system of coordinates has origin at the center of the array, and range axis z orthogonal to it. Then, the transducer locations are $\vec{\mathbf{x}}_r = (\mathbf{x}_r, 0)$, with cross-range $\mathbf{x}_r \in \mathcal{A}$ satisfying $|\mathbf{x}_r| \leq a/2$, for $r = 1, \ldots N$. For convenience, we assume that the center $\vec{\mathbf{y}}^\star$ of the source is on the range axis, at distance L from the array, $\vec{\mathbf{y}}^\star = (\mathbf{0}, L)$. The points $\vec{\mathbf{y}}$ in the search domain $\mathcal{Y}$, where we either observe the time reversed field or we compute the image, are offset from $\vec{\mathbf{y}}^\star$ by $\boldsymbol{\xi}$ in cross-range and by η in range, $\vec{\mathbf{y}} = (\boldsymbol{\xi}, L + \eta)$.

1.2. Model of the array data. With $G(t, \vec{\mathbf{x}}, \vec{\mathbf{y}})$ the Green's function of the wave equation, we get

$$p(t, \vec{\mathbf{x}}_r) = f(t) \star_t \int_{\mathbb{R}^n} d\vec{\mathbf{y}}\, \rho(\vec{\mathbf{y}})\, G(t, \vec{\mathbf{x}}_r, \vec{\mathbf{y}}), \tag{1.3}$$

where $\star_t$ denotes convolution in time. Since it is easier to deal with convolutions in the frequency domain, we use the Fourier transform to write

$$p(t, \vec{\mathbf{x}}_r) = \int_{\infty}^{\infty} \frac{d\omega}{2\pi}\, \widehat{p}(\omega, \vec{\mathbf{x}}_r) e^{-i\omega t}, \qquad \widehat{p}(\omega, \vec{\mathbf{x}}_r) = \widehat{f}(\omega) \int_{\mathbb{R}^d} d\vec{\mathbf{y}}\, \rho(\vec{\mathbf{y}})\, \widehat{G}(\omega, \vec{\mathbf{x}}_r, \vec{\mathbf{y}}), \tag{1.4}$$

with $\widehat{G}(\omega, \vec{\mathbf{x}}, \vec{\mathbf{y}})$ the outgoing Green's function of the Helmholtz equation. The source signal is modeled by

$$f(t) = \cos(\omega_o t) f_B(t), \qquad \widehat{f}(\omega) = \int_{-\infty}^{\infty} d\omega f(t) e^{i\omega t} = \frac{1}{2}\left[\widehat{f}_B(\omega - \omega_o) + \widehat{f}_B(\omega + \omega_o)\right], \tag{1.5}$$

where $f_B(t)$ is a real valued base-band pulse, with Fourier transform $\widehat{f}_B(\omega)$ supported at $\omega \in [-B/2, B/2]$. We call B the *bandwidth* and ω_o the *central frequency*.

The transducers record over a time window $\chi_{_T}(t)$ of duration T. We model it by $\chi_{_T}(t) = T^{-1}\chi\left(t/T\right)$, with the function $\chi(u)$ of dimensionless argument u, compactly supported in the unit interval $[0, 1]$. For example, we may take $\chi(u) = 1_{[0,1]}(u)$, the indicator function equal to one when $u \in [0, 1]$ and zero otherwise.

The model of the array data is $D(t,\vec{\mathbf{x}}_r) = \chi_T(t)p(t,\vec{\mathbf{x}}_r)$, for $r = 1,\dots,N$, with Fourier transform

$$\widehat{D}(\omega,\vec{\mathbf{x}}_r) = \int_{-\infty}^{\infty} d\omega' \, \frac{\widehat{\chi}\,[(\omega-\omega')T]}{2\pi}\widehat{p}(\omega',\vec{\mathbf{x}}_r) = \int_{-\infty}^{\infty} d\omega' \, \frac{\widehat{\chi}\,[(\omega-\omega')T]}{2\pi}\widehat{f}(\omega') \int_{\mathbb{R}^n} d\vec{\mathbf{y}}\, \rho(\vec{\mathbf{y}})\, \widehat{G}(\omega',\vec{\mathbf{x}}_r,\vec{\mathbf{y}}). \quad (1.6)$$

We often call the signals $D(t,\vec{\mathbf{x}}_r)$ *data time traces*, to emphasize that they are functions of time.

1.3. Model of the time reversal function. Each transducer in the array reverses the received signal

$$F(t,\vec{\mathbf{x}}_r) = D(T-t,\vec{\mathbf{x}}_r), \qquad \widehat{F}(\omega,\vec{\mathbf{x}}_r) = \int_{-\infty}^{\infty} dt\, e^{i\omega t} D(T-t,\vec{\mathbf{x}}_r) = \overline{\widehat{D}(\omega,\vec{\mathbf{x}}_r)} e^{i\omega T}, \quad (1.7)$$

and re-emits it in the medium. The acoustic pressure observed at points $\vec{\mathbf{y}} \in \mathcal{Y}$ is

$$p^{\mathrm{TR}}(t,\vec{\mathbf{y}}) = \int_{-\infty}^{\infty} \frac{d\omega}{2\pi}\, e^{-i\omega t} \sum_{r=1}^{N} \widehat{F}(\omega,\vec{\mathbf{x}}_r)\widehat{G}(\omega,\vec{\mathbf{x}}_r,\vec{\mathbf{y}}) = \int_{-\infty}^{\infty} \frac{d\omega}{2\pi}\, e^{i\omega(T-t)} \sum_{r=1}^{N} \overline{\widehat{D}(\omega,\vec{\mathbf{x}}_r)}\widehat{G}(\omega,\vec{\mathbf{x}}_r,\vec{\mathbf{y}}), \quad (1.8)$$

where the bar denotes complex conjugate. It is expected to focus back at the source, at time $t = T$, so we define the time reversal function

$$\mathcal{J}^{\mathrm{TR}}_{\rho,\chi}(\vec{\mathbf{y}}) = p^{\mathrm{TR}}(t=T,\vec{\mathbf{y}}) = \int_{-\infty}^{\infty} \frac{d\omega}{2\pi} \sum_{r=1}^{N} \overline{\widehat{D}(\omega,\vec{\mathbf{x}}_r)}\widehat{G}(\omega,\vec{\mathbf{x}}_r,\vec{\mathbf{y}}). \quad (1.9)$$

The indexes ρ,χ indicate its dependence on the source density ρ and the recording window χ. In the analysis it is usual to assume an ideal point source $\rho(\vec{\mathbf{y}}) = \delta(\vec{\mathbf{y}} - \vec{\mathbf{y}}^\star)$ and an infinite time window $\widehat{\chi}(\omega T) = 2\pi\delta(\omega)$, where $\delta(\cdot)$ is the Dirac delta distribution. It is also usual to make the continuum array aperture approximation (1.2) and forget the scaling factor h^{n-1}. The time reversal function becomes under these simplifications,

$$\mathcal{J}^{\mathrm{TR}}(\vec{\mathbf{y}}) = \int_{-\infty}^{\infty} \frac{d\omega}{2\pi}\, \overline{\widehat{f}(\omega)} \int_{\mathcal{A}} d\mathbf{x}\, \overline{\widehat{G}(\omega,\vec{\mathbf{x}},\vec{\mathbf{y}}^\star)}\widehat{G}(\omega,\vec{\mathbf{x}},\vec{\mathbf{y}}), \qquad \vec{\mathbf{x}} = (\mathbf{x},0). \quad (1.10)$$

1.4. Reverse time migration and the least squares approach to imaging. The least squares estimate $\rho^{\mathrm{LS}}(\vec{\mathbf{x}})$ of the source density is the minimizer of the array data misfit

$$\min_{\rho\in L^2(\mathbb{R}^n)} \mathcal{O}(\rho), \quad \mathcal{O}(\rho) = \langle \mathcal{M}\rho - D, \mathcal{M}\rho - D\rangle = \int_{-\infty}^{\infty} \frac{d\omega}{2\pi} \sum_{r=1}^{N} \left| [\mathcal{M}\rho]\,(\omega,\vec{\mathbf{x}}_r) - \widehat{D}(\omega,\vec{\mathbf{x}}_r)\right|^2. \quad (1.11)$$

Here we assume a square integrable ρ, and let $\mathcal{M}$ be the forward operator that takes ρ to the Hilbert space of the data, with inner product denoted by $\langle\cdot,\cdot\rangle$. We have, similar to (1.6),

$$[\mathcal{M}\rho](\omega,\vec{\mathbf{x}}_r) = \int_{-\infty}^{\infty} d\omega' \, \frac{\widehat{\chi}\,[(\omega-\omega')T]}{2\pi}\widehat{f}(\omega') \int_{\mathbb{R}^n} d\vec{\mathbf{y}}\, \rho(\vec{\mathbf{y}})\, \widehat{G}_o(\omega',\vec{\mathbf{x}}_r,\vec{\mathbf{y}}), \quad (1.12)$$

where $\widehat{G}_o$ is the outgoing Green's function of the Helmholtz equation in the medium with wave speed $c_o(\vec{\mathbf{x}})$, our estimate of the true wave speed $c(\vec{\mathbf{x}})$. We assume henceforth, for simplicity, $\widehat{\chi}(\omega T) = 2\pi\delta(\omega)$.

The least squares solution solves the normal equations $[\mathcal{M}^\star\mathcal{M}\rho^{\mathrm{LS}}](\vec{\mathbf{y}}) = [\mathcal{M}^\star D](\vec{\mathbf{y}})$, where $\mathcal{M}^\star$ is the adjoint operator, that takes the data to the Hilbert space $L^2(\mathbb{R}^n)$,

$$[\mathcal{M}^\star D](\vec{\mathbf{y}}) = \int_{-\infty}^{\infty} \frac{d\omega}{2\pi}\, \widehat{f}(\omega) \sum_{r=1}^{N} \overline{\widehat{D}(\omega,\vec{\mathbf{x}}_r)}\widehat{G}_o(\omega,\vec{\mathbf{x}}_r,\vec{\mathbf{y}}). \quad (1.13)$$

The normal operator $\mathcal{M}^\star\mathcal{M} : L^2(\mathbb{R}^n) \to L^2(\mathbb{R}^n)$ is given by $[\mathcal{M}^\star\mathcal{M}\rho](\vec{\mathbf{y}}) = \int_{\mathbb{R}^n} d\vec{\mathbf{y}}'\, \rho(\vec{\mathbf{y}}')\mathcal{K}(\vec{\mathbf{y}},\vec{\mathbf{y}}')$, with kernel

$$\mathcal{K}(\vec{\mathbf{y}},\vec{\mathbf{y}}') = \int_{-\infty}^{\infty} \frac{d\omega}{2\pi} \left|\widehat{f}(\omega)\right|^2 \sum_{r=1}^{N} \overline{\widehat{G}_o(\omega,\vec{\mathbf{x}}_r,\vec{\mathbf{y}}')}\widehat{G}_o(\omega,\vec{\mathbf{x}}_r,\vec{\mathbf{y}}). \quad (1.14)$$

Note that $\mathcal{K}(\vec{\mathbf{y}},\vec{\mathbf{y}}')$ is the time reversal function for a point source at $\vec{\mathbf{y}}'$ that emits a signal with Fourier transform $|\widehat{f}(\omega)|^2$, in the *smooth, fictitious medium* with wave speed $c_o(\vec{\mathbf{x}})$. It peaks at $\vec{\mathbf{y}}=\vec{\mathbf{y}}'$, and it is large in a vicinity of $\vec{\mathbf{y}}'$, as described by the resolution limits given in section 2. This implies that the right hand side in the normal equations is large around the support of $\rho^{\text{LS}}(\vec{\mathbf{x}})$, and thus it defines an imaging function

$$\mathcal{J}^{\text{M}}(\vec{\mathbf{y}}) = [\mathcal{M}^\star D](\vec{\mathbf{y}}) = \int_{-\infty}^{\infty} \frac{d\omega}{2\pi} \widehat{f}(\omega) \sum_{r=1}^{N} \overline{\widehat{D}(\omega,\vec{\mathbf{x}}_r)} \widehat{G}_o(\omega,\vec{\mathbf{x}}_r,\vec{\mathbf{y}}), \tag{1.15}$$

known as *reverse time migration*. Often, the factor $\widehat{f}(\omega)$ is neglected, because it does not play a big role when the signal $f(t)$ is a pulse. However, for long signals like chirps [Curlander and McDonough, 1991, Section 3.1.2], the factor is important. Explicitly, the convolution of $f(t)$ with $f(-t)$ compresses these signals as if the sources emitted a pulse. The Fourier transform of $f(-t)\star_t f(t)$ is $|\widehat{f}(\omega)|^2$, as it appears in (1.14).

Reverse time migration is common in geophysics [Biondi, 2006], radar [Curlander and McDonough, 1991] and elsewhere, but most often it is replaced by its simplified version known as *Kirchhoff migration*

$$\mathcal{J}^{\text{KM}}(\vec{\mathbf{y}}) = \int_{-\infty}^{\infty} \frac{d\omega}{2\pi} \sum_{r=1}^{N} \widehat{D}(\omega,\vec{\mathbf{x}}_r) e^{-i\omega\tau(\vec{\mathbf{x}}_r,\vec{\mathbf{y}})} = \sum_{r=1}^{N} D(\tau(\vec{\mathbf{x}}_r,\vec{\mathbf{y}}),\vec{\mathbf{x}}_r). \tag{1.16}$$

The simplification uses the high frequency, geometrical optics approximation of the Green's function

$$\widehat{G}_o(\omega,\vec{\mathbf{x}},\vec{\mathbf{y}}) \approx \alpha(\omega_o,L) e^{i\omega\tau(\vec{\mathbf{x}},\vec{\mathbf{y}})}, \tag{1.17}$$

with approximately constant amplitude α, under the assumptions $|\xi|,a,\eta \ll L$. The travel time $\tau(\vec{\mathbf{x}},\vec{\mathbf{y}})$ is given by Fermat's principle, $\tau(\vec{\mathbf{x}},\vec{\mathbf{y}}) = \min \int dl\, c^{-1}(\vec{\mathbf{r}}(l))$, where the minimum is over all paths $\vec{\mathbf{r}}(l)$ parametrized by $l\in\mathbb{R}$, that start at $\vec{\mathbf{y}}$ and end at $\vec{\mathbf{x}}$.

1.5. Coherent interferometric imaging. Equations (1.15-1.16) show how migration forms images by superposing the data traces $D(t,\vec{\mathbf{x}}_r)$ back-propagated to $\vec{\mathbf{y}}\in\mathcal{Y}$, either with the Green's function $\widehat{G}_o$ or with the travel time τ. The *coherent interferometric* (CINT) imaging approach introduced in [Borcea et al., 2005, Borcea et al., 2006] back-propagates to $\vec{\mathbf{y}}\in\mathcal{Y}$ local cross-correlations of the data traces at nearby receivers, instead of the traces themselves. The *local cross-correlations* are defined by

$$\begin{aligned}\mathcal{C}(t,\Delta t,\vec{\mathbf{x}}_r,\vec{\mathbf{x}}_{r'};T_{\mathcal{C}}) &= \int_{\infty}^{\infty} dt'\, \phi_{\mathcal{C}}(t') D\left(t+\frac{\Delta t}{2}-t',\vec{\mathbf{x}}_r\right) D\left(t-\frac{\Delta t}{2}-t',\vec{\mathbf{x}}_{r'}\right) \\ &= \int_{-\infty}^{\infty} \frac{d\omega}{2\pi} e^{-i\omega\Delta t} \int_{-\infty}^{\infty} \frac{d\widetilde{\omega}}{2\pi} e^{-i\widetilde{\omega}t}\, \widehat{\phi}(\widetilde{\omega}T_{\mathcal{C}})\, \widehat{D}\left(\omega+\frac{\widetilde{\omega}}{2},\vec{\mathbf{x}}_r\right) \overline{\widehat{D}\left(\omega-\frac{\widetilde{\omega}}{2},\vec{\mathbf{x}}_{r'}\right)}. \end{aligned} \tag{1.18}$$

They are computed over a time window $\phi_{\mathcal{C}}(t)$ of width $T_{\mathcal{C}}$, modeled by $\phi_{\mathcal{C}}(t) = T_{\mathcal{C}}^{-1}\phi\left(t/T_{\mathcal{C}}\right)$, using the function $\phi(u)$ of dimensionless argument u, and compactly supported at $|u|\le 1/2$.

Let us assume for simplicity that the high frequency, geometrical optics approximation (1.17) applies. The mathematical model of the CINT imaging function is

$$\begin{aligned}\mathcal{J}^{\text{CINT}}(\vec{\mathbf{y}};T_{\mathcal{C}},X_{\mathcal{C}}) = \int_{-\infty}^{\infty} \frac{d\omega}{2\pi} \int_{-\infty}^{\infty} \frac{d\widetilde{\omega}}{2\pi}\, \widehat{\phi}(\widetilde{\omega}T_{\mathcal{C}}) \sum_{r,r'=1}^{N} \psi\left(\frac{|\vec{\mathbf{x}}_r-\vec{\mathbf{x}}_{r'}|}{X_{\mathcal{C}}(\omega)}\right) \widehat{D}\left(\omega+\frac{\widetilde{\omega}}{2},\vec{\mathbf{x}}_r\right) \overline{\widehat{D}\left(\omega-\frac{\widetilde{\omega}}{2},\vec{\mathbf{x}}_{r'}\right)} \times \\ \exp\left\{-i\omega\left[\tau(\vec{\mathbf{x}}_r,\vec{\mathbf{y}})-\tau(\vec{\mathbf{x}}_{r'},\vec{\mathbf{y}})\right] - i\widetilde{\omega}\,\frac{\left[\tau(\vec{\mathbf{x}}_r,\vec{\mathbf{y}})+\tau(\vec{\mathbf{x}}_{r'},\vec{\mathbf{y}})\right]}{2}\right\}. \end{aligned} \tag{1.19}$$

Note how it superposes the local cross-correlations (1.18) back-propagated to $\vec{\mathbf{y}}$ by evaluating them at the mean travel time $t=\left[\tau(\vec{\mathbf{x}}_r,\vec{\mathbf{y}})+\tau(\vec{\mathbf{x}}_{r'},\vec{\mathbf{y}})\right]/2$, and at the difference travel time $\Delta t = \tau(\vec{\mathbf{x}}_r,\vec{\mathbf{y}})-\tau(\vec{\mathbf{x}}_{r'},\vec{\mathbf{y}})$. Note also that we introduced another window function $\psi(u)$, supported at $|u|\le 1/2$. Its purpose is to restrict the superposition in (1.19) to the receivers that are not further than the distance $X_{\mathcal{C}}(\omega)$ apart. In general, this distance may vary in the bandwidth.

2. Resolution and robustness of time reversal and imaging in random media. The performance of the time reversal and imaging processes is assessed by their *resolution* and *robustness.* The *resolution* quantifies the ability of the process to distinguish between two localized sources. We analyze it by estimating the support of the point-spread function, the model of the process for a point-like source. The models derived above are random, because the waves travel from the source to the array in a random medium. Therefore, we quantify the resolution using the mean (statistical expectation) of the models.

A *robust* process gives a high signal-to-noise (SNR) ratio. Recall that we look for the peaks of the random functions that model time reversal and imaging. By high SNR we mean that these peaks are insensitive to the noise and are clearly distinguishable. Usually, one considers additive, uncorrelated, instrument noise in the data. Here we consider *clutter noise* due to scattering of the waves in the medium. It is not additive, it has a complex structure, it exhibits correlations across the array and over frequencies, and it is much harder to mitigate than instrument noise. The high SNR of imaging (or time reversal) in random media means that the random fluctuation of the images (or wave field) induced by the clutter noise, are small and therefore, the results are insensitive to the particular realization of the random medium. Such robustness is called *statistical stability* [Papanicolaou et al., 2004, Borcea et al., 2007, Blomgren et al., 2002] and it is an essential quality of any useful method in random media.

2.1. Resolution. For simplicity, we use the continuum array approximation (1.2), and assume that the background medium is homogeneous, with constant wave speed c_o. The Green's function is approximated by (1.17), with $\tau(\vec{\mathbf{x}},\vec{\mathbf{y}}) = |\vec{\mathbf{x}}-\vec{\mathbf{y}}|/c_o$. We have a point source at $\vec{\mathbf{y}}^\star$.

To quantify the resolution, we estimate the support of the mean point spread functions of time reversal, KM and CINT. We need the first and second statistical moments of the random Greens' function $\widehat{G}(\omega,\vec{\mathbf{x}},\vec{\mathbf{y}})$. The details of the calculation of these moments depend on the particular model of the fluctuations $\mu(\vec{\mathbf{x}})$. For *mixing, isotropic* fluctuations, that is fluctuations with integrable correlation function $\mathbb{R}(\vec{\mathbf{x}}) = \mathbb{R}(|\vec{\mathbf{x}}|)$, the moments have the generic form

$$\mathbb{E}\left\{\widehat{G}(\omega,\vec{\mathbf{x}},\vec{\mathbf{y}}^\star)\right\} \approx \widehat{G}_o(\omega,\vec{\mathbf{x}},\vec{\mathbf{y}}^\star)\exp\left[-\frac{\omega^2}{2\Omega_d^2}\right] \approx \alpha(\omega_o,L)\exp\left[i\omega\tau(\vec{\mathbf{x}},\vec{\mathbf{y}}^\star) - \frac{\omega^2}{2\Omega_d^2}\right], \tag{2.1}$$

$$\mathbb{E}\left\{\widehat{G}\left(\omega+\frac{\widetilde{\omega}}{2},\left(\mathbf{x}+\frac{\widetilde{\mathbf{x}}}{2},0\right),\vec{\mathbf{y}}^\star\right)\overline{\widehat{G}\left(\omega-\frac{\widetilde{\omega}}{2},\left(\mathbf{x}-\frac{\widetilde{\mathbf{x}}}{2},0\right),\vec{\mathbf{y}}^\star\right)}\right\} \approx |\alpha(\omega_o,L)|^2 \times$$
$$\exp\left[i\omega\Delta\tau(\mathbf{x},\widetilde{\mathbf{x}},\vec{\mathbf{y}}^\star) + i\widetilde{\omega}\bar{\tau}(\mathbf{x},\widetilde{\mathbf{x}},\vec{\mathbf{y}}^\star) - \frac{\widetilde{\omega}^2}{2\Omega_d^2} - \frac{|\widetilde{\mathbf{x}}|^2}{2X_d^2(\omega)}\right], \tag{2.2}$$

where we let

$$\bar{\tau}(\mathbf{x},\widetilde{\mathbf{x}},\vec{\mathbf{y}}) = \frac{\tau\left[\left(\mathbf{x}+\frac{\widetilde{\mathbf{x}}}{2},0\right),\vec{\mathbf{y}}\right]+\tau\left[\left(\mathbf{x}-\frac{\widetilde{\mathbf{x}}}{2},0\right)\right),\vec{\mathbf{y}}\right]}{2}, \quad \Delta\tau(\mathbf{x},\widetilde{\mathbf{x}},\vec{\mathbf{y}}) = \tau\left[\left(\mathbf{x}+\frac{\widetilde{\mathbf{x}}}{2},0\right),\vec{\mathbf{y}}\right]-\tau\left[\left(\mathbf{x}-\frac{\widetilde{\mathbf{x}}}{2},0\right),\vec{\mathbf{y}}\right].$$

We refer the reader to [Borcea et al., 2005, Appendix B] for the derivation of these formulas in the random paraxial (forward scattering) regime, in which $\lambda_o \ll a \ll L$ and the random fluctuations are small $\gamma \ll 1$, with correlation length ℓ (typical size of the inhomogeneities) satisfying $\ell \ll L$. See also [Borcea et al., 2011, Lemma 3.2] for the derivation of the same moment formulas, under a much simpler model of the random fluctuations, that gives only random wave front distortions.

The first moment formula (2.1) says that the mean field is exponentially damped. There is no absorption in our model. The damping means that the wave field loses coherence because of scattering in the medium, and the incoherent field $\widehat{G} - E\{\widehat{G}\}$ becomes the dominant part of $\widehat{G}$. The second moment formula (2.2) says that the wave fields are statistically correlated over frequency offsets satisfying $|\widetilde{\omega}| \lesssim \Omega_d$ and over transducer offsets $\widetilde{\mathbf{x}}$ satisfying $|\widetilde{\mathbf{x}}| \lesssim X_d(\omega)$. We call Ω_d the *decoherence frequency* and $X_d(\omega)$ the *decoherence length.*

Their precise expressions are model dependent, but they are in general determined by the correlation function $\mathbb{R}(|\vec{\mathbf{x}}|)$, and they decrease with range L. The decoherence length is also proportional to the wavelength $\lambda = 2\pi c_o/\omega$, and we write it in the form $X_d(\omega) = \frac{\lambda L}{a_e(L)}$, with $a_e(L)$ having units of length, and increasing with range. It is called in [Borcea et al., 2005, Blomgren et al., 2002] the *effective aperture* for the reasons explained below.

The resolution study is simpler in the Fraunhofer diffraction regime [Born and Wolf, 1999], where $a \ll L$ and the Fresnel number $a^2/(\lambda L)$ is small. It allows us to linearize phases in the models of time reversal and imaging, and obtain simpler expressions that can be interpreted as decompositions in plane waves.

2.1.1. Cross-range resolution. Consider search points $\vec{\mathbf{y}}$ that are offset from the source location only in cross-range: $\vec{\mathbf{y}} = (\boldsymbol{\xi}, L)$. The expectation of the time reversal function is

$$\mathbb{E}\{\mathcal{J}^{\rm TR}(\boldsymbol{\xi}, L)\} \approx |\alpha(\omega_o)L|^2 \int_{-\infty}^{\infty} \overline{\widehat{f}(\omega)} \int_{\mathcal{A}} d\mathbf{x}\, \exp\left\{ i\omega \left[\tau(\vec{\mathbf{x}}, \vec{\mathbf{y}}) - \tau(\vec{\mathbf{x}}, \vec{\mathbf{y}}^\star)\right] - \frac{|\boldsymbol{\xi}|^2}{2X_d^2(\omega)} \right\} \tag{2.3}$$

and we obtain with the approximation $\tau(\vec{\mathbf{x}}, \vec{\mathbf{y}}) - \tau(\vec{\mathbf{x}}, \vec{\mathbf{y}}^\star) \approx \boldsymbol{\xi} \cdot \nabla_{\mathbf{y}} \tau(\vec{\mathbf{x}}, \vec{\mathbf{y}}^\star) \approx -\frac{\boldsymbol{\xi}\cdot\mathbf{x}}{c_o L}$, that

$$\mathbb{E}\{\mathcal{J}^{\rm TR}(\boldsymbol{\xi}, L)\} \approx |\alpha(\omega_o)L|^2 a^{n-1} \int_{-\infty}^{\infty} \overline{\widehat{f}(\omega)} e^{-\frac{|\boldsymbol{\xi}|^2}{2X_d^2(\omega)}} \prod_{j=1}^{n-1} \mathrm{sinc}\left(\frac{\pi a \xi_j}{\lambda L}\right). \tag{2.4}$$

Here ξ_j are the components of vector $\boldsymbol{\xi}$ and $\mathrm{sinc}(u) = \sin(u)/u$. The expectation of the KM function is

$$\begin{aligned}
\mathbb{E}\{\mathcal{J}^{\rm KM}(\boldsymbol{\xi}, L)\} &= \int_{-\infty}^{\infty} \frac{d\omega}{2\pi}\, \widehat{f}(\omega) \int_{\mathcal{A}} d\mathbf{x}\, \mathbb{E}\{\widehat{G}(\omega, \vec{\mathbf{x}}, \vec{\mathbf{y}}^\star)\} e^{-i\omega\tau(\vec{\mathbf{x}}, \vec{\mathbf{y}})} \\
&\approx \alpha(\omega_o, L) a^{n-1} \int_{-\infty}^{\infty} \widehat{f}(\omega) e^{-\frac{\omega^2}{2\Omega_d^2}} \prod_{j=1}^{n-1} \mathrm{sinc}\left(\frac{\pi a \xi_j}{\lambda L}\right).
\end{aligned} \tag{2.5}$$

The expectation of the CINT function is more complicated

$$\begin{aligned}
\mathbb{E}\{\mathcal{J}^{\rm CINT}(\boldsymbol{\xi}, L)\} \approx |\alpha(\omega_o, L)|^2 \int_{-\infty}^{\infty} \frac{d\omega}{2\pi} \int_{-\infty}^{\infty} \frac{d\widetilde{\omega}}{2\pi} \overline{\widehat{f}\left(\omega + \frac{\widetilde{\omega}}{2}\right)} \widehat{f}\left(\omega - \frac{\widetilde{\omega}}{2}\right) \widehat{\phi}(\widetilde{\omega} T_c) \int_{\mathcal{A}} d\mathbf{x} \int_{\mathbb{R}^{n-1}} d\widetilde{\mathbf{x}}\, \psi\left(\frac{|\widetilde{\mathbf{x}}|}{X_c(\omega)}\right) \times \\
\exp\left\{ i\widetilde{\omega}\left[\bar{\tau}(\mathbf{x}, \widetilde{\mathbf{x}}, \vec{\mathbf{y}}^\star) - \bar{\tau}(\mathbf{x}, \widetilde{\mathbf{x}}, \vec{\mathbf{y}})\right] + i\omega\left[\Delta\tau(\mathbf{x}, \widetilde{\mathbf{x}}, \vec{\mathbf{y}}^\star) - \Delta\tau(\mathbf{x}, \widetilde{\mathbf{x}}, \vec{\mathbf{y}})\right] - \frac{\widetilde{\omega}^2}{2\Omega_d^2} - \frac{|\widetilde{\mathbf{x}}|^2}{2X_d^2(\omega)} \right\}.
\end{aligned} \tag{2.6}$$

We can simplify it by assuming: (1) A small X_d (i.e., a small $|\widetilde{\mathbf{x}}|$), so that $\bar{\tau}(\mathbf{x}, \widetilde{\mathbf{x}}, \vec{\mathbf{y}}) \approx \tau(\vec{\mathbf{x}}, \vec{\mathbf{y}})$ and $\Delta\tau(\mathbf{x}, \widetilde{\mathbf{x}}, \vec{\mathbf{y}}^\star) \approx \widetilde{\mathbf{x}} \cdot \nabla_{\mathbf{x}} \tau(\vec{\mathbf{x}}, \vec{\mathbf{y}}) \approx \frac{\widetilde{\mathbf{x}}\cdot(\mathbf{x}-\boldsymbol{\xi})}{L}$. (2) A small Ω_d (i.e., a small $|\widetilde{\omega}|$) and a smooth pulse, so that $\widehat{f}(\omega \pm \widetilde{\omega}/2) \approx \widehat{f}(\omega)$. (3) The windows $\widehat{\phi}(\widetilde{\omega} T_c)$ and $\psi(|\widetilde{\mathbf{x}}|/X_c)$ are one in the essential support of the Gaussians in $\widetilde{\omega}$ and $\widetilde{\mathbf{x}}$ in (2.6) and zero outside. We obtain after some straightforward calculations

$$\mathbb{E}\{\mathcal{J}^{\rm CINT}(\boldsymbol{\xi}, L)\} \approx (2\pi)^{\frac{n}{2}-1} \Omega_d\, |\alpha(\omega_o, L)|^2 \left[\frac{a\,L}{a_e(L)}\right]^{n-1} \int_{-\infty}^{\infty} \frac{d\omega}{2\pi}\, |\widehat{f}(\omega)|^2 \lambda^{n-1}\, \exp\left[-\frac{2\pi^2 |\boldsymbol{\xi}|^2}{a_e^2(L)}\right]. \tag{2.7}$$

Conclusions: Equations (2.4), (2.5) and (2.7) show that the mean time reversal and imaging functions peak at the true source location, i.e., at $\boldsymbol{\xi} = \mathbf{0}$. However, they have different resolution. The resolution of KM is the same as that in the homogeneous medium. It is defined as the distance between the peak of the sinc function and its first zero, and it is given by the Rayleigh resolution formula [Born and Wolf, 1999]

$$\frac{\lambda_o L}{a}\left[1 + O\left(\frac{B}{\omega_o}\right)\right] \approx \frac{\lambda_o L}{a}, \qquad \text{if } B \ll \omega_o. \tag{2.8}$$

The resolution of time reversal is *better*, assuming that $a_e(L) > a$,

$$|\boldsymbol{\xi}| \lesssim X_d(\omega) = \frac{\lambda_o L}{a_e(L)}\left[1 + O\left(\frac{B}{\omega_o}\right)\right] \approx \frac{\lambda_o L}{a_e(L)}. \tag{2.9}$$

This happens when the cumulative wave scattering in the random medium is strong and causes the waves to decorrelate over small distances X_d. The improved cross-range focusing is called *super-resolution*. It was discovered and demonstrated experimentally in [Fink, 1997], and has been explained theoretically in terms of the enhanced effective aperture $a_e(L)$ in [Blomgren et al., 2002, Borcea et al., 2005, Papanicolaou et al., 2004]. The resolution of CINT is proportional to the effective aperture $|\boldsymbol{\xi}| \lesssim \frac{a_e(L)}{2\pi}$ and thus, it *deteriorates as wave scattering becomes stronger*.

2.1.2. Range resolution. When the search points $\vec{\mathbf{y}} = (\mathbf{0}, L+\eta)$ are offset only in range from $\vec{\mathbf{y}}^\star$,

$$\mathbb{E}\{\mathcal{J}^{\rm TR}(\mathbf{0}, L+\eta)\} \approx |\alpha(\omega_o, L)|^2 a^{n-1} \int_{-\infty}^{\infty} \frac{d\omega}{2\pi} \overline{\widehat{f}(\omega)} \exp\left(-\frac{\omega^2}{2\Omega_d^2}\frac{\eta}{L} + i\frac{\omega}{c_o}\eta\right). \tag{2.10}$$

Here we used the moment formula [Borcea et al., 2005, Appendix B]

$$\mathbb{E}\left\{\overline{\widehat{G}\,(\omega, \vec{\mathbf{x}}, \vec{\mathbf{y}}^\star)}\widehat{G}\,(\omega, \vec{\mathbf{x}}, \vec{\mathbf{y}})\right\} \approx \overline{\widehat{G}_o\,(\omega, \vec{\mathbf{x}}, \vec{\mathbf{y}}^\star)}\widehat{G}_o\,(\omega, \vec{\mathbf{x}}, \vec{\mathbf{y}}) \exp\left(-\frac{\omega^2}{2\Omega_d^2}\frac{\eta}{L}\right), \tag{2.11}$$

and the approximation $\tau(\vec{\mathbf{x}}, \vec{\mathbf{y}}) - \tau(\vec{\mathbf{x}}, \vec{\mathbf{y}}^\star) \approx \eta/c_o$. For the KM function we get

$$\mathbb{E}\{\mathcal{J}^{\rm KM}(\mathbf{0}, L+\eta)\} \approx \alpha(\omega_o, L) a^{n-1} \int_{-\infty}^{\infty} \frac{d\omega}{2\pi} \widehat{f}(\omega) \exp\left(-\frac{\omega^2}{2\Omega_d^2} - i\frac{\omega}{c_o}\eta\right), \tag{2.12}$$

and for CINT

$$\mathbb{E}\{\mathcal{J}^{\rm CINT}(\mathbf{0}, L+\eta)\} \approx (2\pi)^{\frac{n}{2}-1}\Omega_d |\alpha(\omega_o, L)|^2 \left[\frac{a\,L}{a_e(L)}\right]^{n-1} \int_{-\infty}^{\infty} \frac{d\omega}{2\pi} |\widehat{f}(\omega)|^2 \lambda^{n-1} \exp\left[-\frac{\eta^2}{2(c_o/\Omega_d)^2}\right]. \tag{2.13}$$

Conclusions: All the mean functions peak at the source location, where $\eta = 0$, but they have different resolution. The range resolution of time reversal is

$$|\eta| \lesssim \min\left\{\frac{c_o}{B}, L\left(\frac{\Omega_d}{\omega_o}\right)^2\right\}. \tag{2.14}$$

In most regimes it is comparable to that of the mean KM function, $|\eta| \lesssim c_o/B$, determined by the pulse bandwidth. However, the range resolution of CINT is worse in random media, where cumulative wave scattering causes wave decorrelation over frequency offsets $\Omega_d < B$. We have $|\eta| \lesssim c_o/\Omega_d$.

2.2. Statistical stability. There is another fundamental difference between time reversal, KM and CINT imaging. Note how the mean KM function at the peak is exponentially damped because of the factor $\exp[-\omega^2/(2\Omega_d^2)]$. In random media, where $\Omega_d \ll \omega_o$, this is typically almost zero. The magnitude of the random fluctuations of $\mathcal{J}^{\rm KM}(\vec{\mathbf{y}})$ are determined by its standard deviation $\sigma^{\rm KM}(\vec{\mathbf{y}})$. Its calculation involves the second moments (2.2) of the Green's function and it is similar to that of computing $\mathbb{E}\{\mathcal{J}^{\rm CINT}\}$. The SNR is the ratio $\mathbb{E}\{\mathcal{J}^{\rm KM}(\vec{\mathbf{y}}^\star)\}/\sigma^{\rm KM}(\vec{\mathbf{y}}^\star)$. It is exponentially small, of the order $\exp[-\omega_o^2/(2\Omega_d^2)]$, no matter how large the array aperture is. If we had uncorrelated, additive noise, the SNR would improve for larger arrays, because the noise would be averaged out by the superposition over the many sensors. The random medium noise is much more complex and in general it cannot be removed by simply increasing the array aperture. The KM method is not useful in imaging in random media, because the signal, the value of the function at the expected peak $\vec{\mathbf{y}}^\star$ is faint and not distinguishable from the noise, the random fluctuations of the image.

The mean time reversal and CINT functions are not exponentially damped as KM is. This is key to their robustness. Examples of proofs of the statistical stability of time reversal and CINT imaging are in [Papanicolaou et al., 2004] and in [Borcea et al., 2007], respectively. They assume a paraxial, forward scattering regime, and certain asymptotic limits, and show that $\mathcal{J}^{\rm TR}(\vec{\mathbf{y}})$ and $\mathcal{J}^{\rm CINT}(\vec{\mathbf{y}})$ converge in probability to a deterministic limit. A more quantitative statistical stability study requires the calculation of the SNR,

which is much more difficult than for KM, because it involves fourth order moments of the Green's function. The SNR of CINT has been calculated only recently in [Borcea et al., 2011], for a simple model of the random medium that gives only random wave front distortions, but does not account for multiple wave scattering. The result in [Borcea et al., 2011] shows that the SNR of CINT is large and it can be improved by increasing the array aperture.

Note that statistical stability of time reversal typically holds only in broadband [Blomgren et al., 2002]. The stability of CINT is also in broadband and subject to choosing the proper time and transducer offset thresholds T_c and X_c in (1.19). In section 2 we made the optimal choice with thresholds given by the decoherence frequency and length, $1/T_c = \Omega_d$ and $X_c = X_d$. If we chose $1/T_c > \Omega_d$ and $X_c > X_d$ instead, the resolution analysis would have stayed the same, but the stability result would not hold. It turns out the thresholding by T_c and X_c has a statistical smoothing effect [Borcea et al., 2007] and it is essential for a robust CINT imaging process. The smoothing comes at the expense of loss of resolution. If we chose $1/T_c < \Omega_d$ and $X_c < X_d$, the resolution of CINT would be worse, by a factor X_d/X_c in cross-range and $T_c\Omega_d$ in range. This trade-off between resolution and stability in CINT can be used to determine the optimal thresholding parameters T_c, X_c, without apriori knowledge about the statistics of the medium, that is about Ω_d and X_d. This is the idea of the adaptive CINT algorithm introduced and studied in [Borcea et al., 2006].

3. Summary. We have described the fundamental differences between the time reversal process and imaging in random media. Wave scattering may lead to *super-resolution* of time reversal [Fink, 1997], but this is not useful in imaging. Traditional imaging methods, like reverse time migration cannot be used for robust imaging in random media. Coherent interferometry can give robust results, but its resolution deteriorates as the cumulative wave scattering effects increase. CINT by itself will not work in strong scattering media, but in some cases it can be complemented with additional data pre-processing designed to filter out clutter effects [Borcea et al., 2010, Alonso et al., 2011]. We discussed only imaging with passive arrays, because it is the natural setting for comparison with time reversal. We refer to [Borcea et al., 2006, Borcea et al., 2011] for studies of CINT imaging of scatterers with active arrays.

REFERENCES

[Alonso et al., 2011] Alonso, R., Borcea, L., Papanicolaou, G., and Tsogka, C. (2011). Detection and imaging in strongly backscattering randomly layered media. *Inverse Problems*, 27:025004.

[Biondi, 2006] Biondi, B. (2006). *3D seismic imaging*. Society of Exploration Geophysicists.

[Blomgren et al., 2002] Blomgren, P., Papanicolaou, G., and Zhao, H. (2002). Super-resolution in time-reversal acoustics. *The Journal of the Acoustical Society of America*, 111:230.

[Borcea et al., 2010] Borcea, L., del Cueto, F., Papanicolaou, G., and Tsogka, C. (2010). Filtering random layering effects in imaging. *SIAM Multiscale Modeling and Simulation*, 8:751–781.

[Borcea et al., 2011] Borcea, L., Garnier, J., Papanicolaou, G., and Tsogka, C. (submitted 2011). Enhanced statistical stability in coherent interferometric imaging. *submitted, Inverse Problems*.

[Borcea et al., 2005] Borcea, L., Papanicolaou, G., and Tsogka, C. (2005). Interferometric array imaging in clutter. *Inverse Problems*, 21:1419–1460.

[Borcea et al., 2006] Borcea, L., Papanicolaou, G., and Tsogka, C. (2006). Adaptive interferometric imaging in clutter and optimal illumination. *Inverse Problems*, 22:1405–1436.

[Borcea et al., 2007] Borcea, L., Papanicolaou, G., and Tsogka, C. (2007). Asymptotics for the space-time Wigner transform with applications to imaging. *Stochastic Differential Equations: Theory and Applications. Volume in Honor of Professor Boris L Rozovskii, PH Baxendale and SV Lototsky editors., Interdisciplinary Mathematical Sciences*, 2.

[Born and Wolf, 1999] Born, M. and Wolf, E. (1999). *Principles of optics: Electromagnetic theory of propagation, interference and diffraction of light*. Cambridge University Press, Cambridge, 7 edition.

[Carazzone and Symes, 1991] Carazzone, J. and Symes, W. (1991). Velocity inversion by differential semblance optimization. *Geophysics*, 56.

[Curlander and McDonough, 1991] Curlander, J. and McDonough, R. (1991). *Synthetic aperture radar- Systems and signal processing(Book)*. New York: John Wiley & Sons, Inc.

[Fink, 1997] Fink, M. (1997). Time reversed acoustics. *Physics Today*, 50:34.

[Papanicolaou et al., 2004] Papanicolaou, G., Ryzhik, L., and Sølna, K. (2004). Statistical stability in time reversal. *SIAM Journal on Applied Mathematics*, 64(4):1133–1155.

[Uhlmann, 2001] Uhlmann, G. (2001). Travel time tomography. *J. Korean Math. Soc*, 38(4):711–722.